A high-energy, high-flux source of gamma-rays from all-optical nonlinear Thomson scattering

Corvan, D. J., Zepf, M., & Sarri, G. (2016). A high-energy, high-flux source of gamma-rays from all-optical nonlinear Thomson scattering. Nuclear Instruments & Methods in Physics Research - Section A: Accelerators, Spectrometers, Detectors, and Associated Equipment, 829, 291-300. DOI: 10.1016/j.nima.2016.03.077

Published in:
Nuclear Instruments & Methods in Physics Research - Section A: Accelerators, Spectrometers, Detectors, and Associated Equipment

Document Version:
Early version, also known as pre-print

A High-Energy, High-Flux Source of Gamma-Rays From All-Optical Non-Linear Thomson Scattering

D. J. Corvan[1], M. Zepf[1], and G. Sarri[1]
[1]*School of Mathematics and Physics, Queens University Belfast, BT7 1NN, Belfast, UK*
(Dated: March 3, 2016)

γ-ray sources are among the most fundamental experimental tools currently available to modern physics. As well as the obvious benefits to fundamental research, an ultra-bright source of γ-rays could form the foundation of scanning of shipping containers for special nuclear materials and provide the bases for new types of cancer therapy.

However, for these applications to prove viable, γ-ray sources must become compact and relatively cheap to manufacture. In recent years, advances in laser technology have formed the cornerstone of optical sources of high energy electrons which already have been used to generate synchrotron radiation on a compact scale. Exploiting the scattering induced by a second laser, one can further enhance the energy and number of photons produced provided the problems of synchronisation and compact γ-ray detection are solved.

Here, we report on the work that has been done in developing an all-optical and hence, compact Non-Linear Thomson Scattering source, including the new methods of synchronisation and compact γ-ray detection. We present evidence of the generation of multi-MeV (maximum $16-18$ MeV) and ultra-high brilliance (exceeding 10^{20} photons s^{-1} mm^{-2} mrad $^{-2}$ 0.1% BW at 15 MeV) γ-ray beams. These characteristics are appealing for the paramount practical applications mentioned above.

I. INTRO

γ-ray sources (energy per photon exceeding the MeV) are one of the most fundamental experimental tools currently available to modern physics thanks to their unique properties in interacting with matter. For instance, nuclear excitations usually have resonances in the MeV range [1], leading to the possible onset of nuclear resonance fluorescence [2] and photofission of materials [3]. These phenomena are of paramount importance, not only for fundamental experimental investigations of nuclear physics, but also for practical applications; for example, the resonances and generated by-products emitted during γ-ray irradiation are distinctive features of each element, and are thus proposed as a viable way of remotely detecting strategic elements even in shielded environments [1].

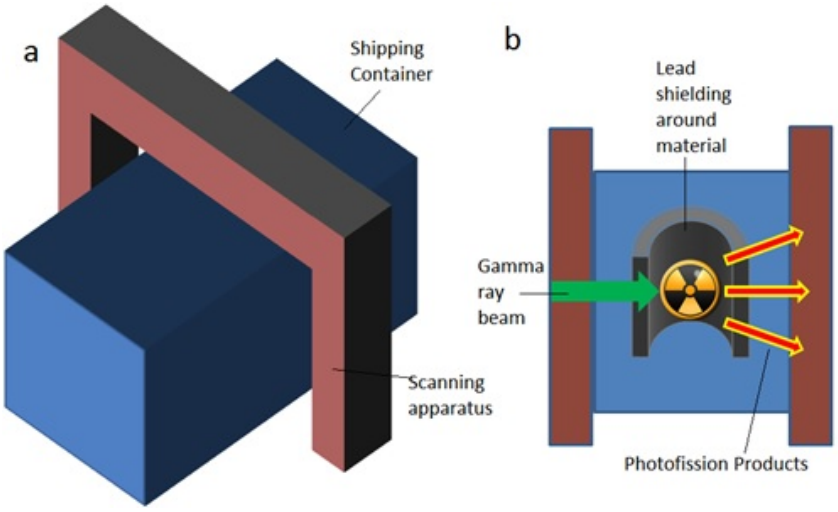

FIG. 1: The basic principle behind the scanning of shipping containers. (a) shows a stylised shipping container moving through a scanning apparatus which is non-invasive. (b) as the gamma rays propagate deep into the container which contains special nuclear material concealed within a lead house, the interact with all of the material inside. Each material responds in a unique way with the emission of specific by-products that can allow one to identify the potentially dangerous material and raise the alarm.

Moreover, their high penetration in materials promotes γ-rays as ideal tools for performing high-quality radiographs of the interior of heavily shielded objects, such as containers and cargos (of which an extremely low faction are currently able to be inspected [4]); allowing one to scan for special nuclear materials such as Uranium−235 such as the example presented in figure 1 (see, for instance, the Container Security Initiative launched by the U.S. Bureau of Customs and Border Protection [5–7]).

As well as scanning, high-energy γ-rays have an impact on living tissues and cells, inducing an extremely complex chain of phenomena in cells ranging from harmless mutations up to cell death. These phenomena are at the core of one of the most effective cancer therapies: radiotherapy [8].

Besides these extremely important practical applications, the detailed study of γ-ray emission represents a precious tool to experimentally access and study physics regimes that would be inaccessible otherwise [9]. For example, the recent development of γ-ray telescopes is allowing for tremendous advances in our understanding of the Universe [10]. In addition, not only can understanding how γ-rays are produced provide insight into astrophysical phenomena but the fast-paced progress of laser technology is now opening up the possibility of experimentally studying quantum electro-dynamics in a highly non-linear regime [11].

II. THE NEED FOR ALL OPTICAL SOURCES OF GAMMA RAYS

There are a number of mechanisms that can produce high-energy γ-rays. Currently the most applied technique involves generating energetic electrons and colliding them with high Z targets, generating 'breaking radiation' called Bremsstrahlung. Figure 2 shows, as an example, the bremsstrahlung spectrum recently obtained from the collision of an energetic laser-driven bunch of electrons with a high Z target [12]. As one can see, the spectrum is extremely broad and while the efficiency for lower energies is high, the number of photons produced towards the higher energies can be seen to decay. Moreover, the photons exiting the target will have a broad divergence and a relatively large spot size, all factors ultimately limiting the brilliance achievable by this source.

Most other sources involve in some regard, the acceleration of charges, specifically electrons, and the subsequent emission of synchrotron radiation [13, 14].

Conventional synchrotrons are large machines which use magnetic fields to guide fast moving electrons around a circular track [15]. This emission can however be enhanced by the use of an undulator or wiggler arrangement. In general, an undulator is a spatially periodic magnetic structure designed to produce a quasi-monoenergetic spectrum of synchrotron radiation from a relativistic bunch of electrons. However, any system that can cause a periodic oscillation of the electron as it propagates can be considered analogus to the original undulator setup. In the context of work presented here, the mechanism driving

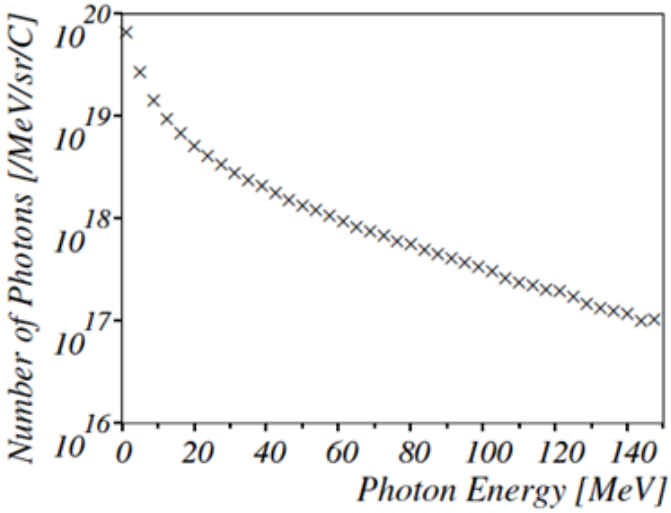

FIG. 2: Bremsstrahlung spectrum from a laser-driven energetic bunch of electrons colliding with a high Z target [12]. Numbers are given per MeV per steradian per Coulomb of charge.

the oscillations will be an intense laser field. Figure 3 shows the characteristic motion of an electron with

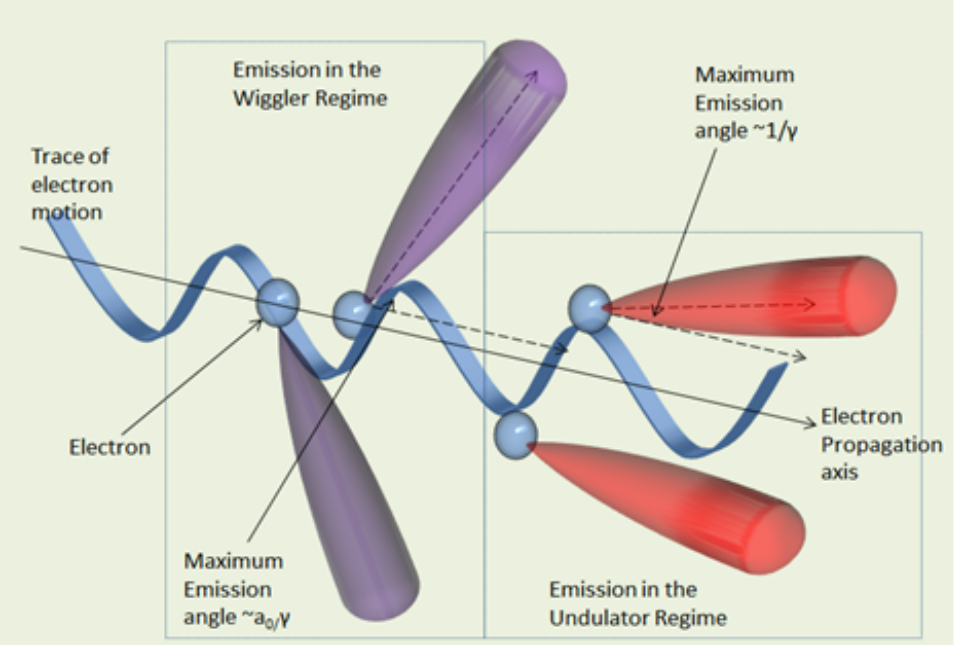

FIG. 3: An electron with velocity β along the z axis undulates with amplitude in the x axis, emits in a cone of angle $1/\gamma$ however, as the oscillations result in a variation in the angle by ψ_0 the opening angle of emitted radiation is changed. The value of ψ_0 determines whether the electron emits in the undulator, or the stronger wiggler regime [13, 16].

velocity $\boldsymbol{\beta}$ (the ratio of electron velocity to the speed of light) which is oscillating as it propagates along the z axis. The restoring acceleration is in the y axis and is given by $\dot{\boldsymbol{\beta}}$. The spatial period of oscillation is given by λ_u. The maximum deflection angle with respect to the z axis is given by ψ_0. The ratio of ψ_0 compared with the natural emission angle $1/\gamma$ gives the undulator strength parameter $K_u = \gamma\psi_0$. If $K_u < 1$ then the value of ψ_0 is lower than the value of the natural opening angle and the system is said to be in the undulator regime. If $K_u > 1$ then the value of ψ_0 is larger than the value of the natural opening angle and the emission is in the wiggler regime [13, 17].

With $\psi_0 < 1/\gamma$, an electron which traverses an undulator setup emits a smoothly modulated field with quasi-monoenergitic properties. In the ultra-relativistic case, it is straightforward to determine the energy of photons emitted in the undulator regime. As the periodicity of the electron in the undulator is given by $2\pi\beta c/\lambda_u = \Omega_u$, the frequency of emitted photons becomes:

$$\omega = \frac{2\gamma^2}{1+\gamma^2\theta^2}\Omega_u \tag{1}$$

The number of photons emitted per electron in an undulator scenario is given as

$$\frac{N_{\gamma u}}{N_{elm}} = \frac{2\pi\alpha K_u^2}{3} \tag{2}$$

Where N_{elm} is the number of undulator elements in the setup, θ is the angle observations are made at with respect to the electron propagation axis and α is the fine structure constant. From this it can be seen that for the undulator regime, there is a squared dependence for the number of photons generated on the undulator strength parameter K_u. Since $K_u < 1$ for an undulator, one can conclude that the emission of photons becomes very low as $K_u \to 0$ [13, 17].

With $\psi_0 > 1/\gamma$, an electron which traverses a wiggler setup is strongly modulated and emits a much broader spectrum which contains many harmonics up to a maximum cut-off energy. This is largely due to the strong field periodically modifying the trajectory of the electron allowing the formation of harmonic

modes. The motion alters equation 1 to

$$\omega_w = m\omega = \frac{2m\gamma^{*2}}{1+\gamma^{*2}\theta^2}\Omega_u \tag{3}$$

where m is the mode number and γ^* is the Lorentz factor modified to take into account the motion of the electron in the transverse direction induced by the action of the wiggler elements. This is the normalised drift velocity β^* i.e., $\gamma^* \approx \gamma/\sqrt{1+K_u^2/2}$.

Clearly it is not possible for the modes to extend to infinity; thus, a critical cut-off frequency must exist. When the electron is at its peak position in x the largest accelerating force is experienced and, the critical frequency becomes

$$\omega_c = \frac{3}{2}K_u\gamma^2 2\pi c/\lambda_u \tag{4}$$

The number of photons produced is given to be

$$\frac{N_{\gamma w}}{N_{elm}} = \frac{5\sqrt{3}\pi\alpha K_u}{6} \tag{5}$$

From this it can be seen that for the wiggler regime, there is a linear dependence for the number of photons generated on the undulator strength parameter K_u. Since $K_u > 1$ for a wiggler, one can conclude that the emission of photons becomes higher $K_u \to \infty$. This will be accompanied by an increase in the angle of emission [13, 17].

In either the wiggler or undulator regimes it can be seen from equations 1 and 3 that increasing the Lorentz factor is critical in order to generate high energy photons, and that a strong K_u is beneficial for gaining further enhancement of those energies. However, using conventional magnets to gain $K_u \gg 1$ can be difficult to achieve due to the engineering constraints imposed. Previously, it was noted that any field with sufficient strength could be used to wiggle the electrons and as laser technology continues to improve and intensities increase, the possibility of accelerating an electron to relativistic velocities in the transverse direction within one laser time period has already been realised. The a_0, or non-linearity parameter is the ratio of the force of the electric field in a single time period to the rest mass of the electron and is used to define the intensity of a laser in terms of this condition.

$$a_0 = \frac{eE_l^2}{m_e\omega_l} \tag{6}$$

Where E_l is the electric field associated with the laser and ω_l is the central frequency of the laser pulse. Above unity, the equation indicates that the magnetic component of the Lorentz force will be comparable to the to the electric field component. The behaviour of the electron becomes highly non-linear. If a laser possesses $a_0 \geq 1$, it is said to be relativistically intense.

In most conventional systems such as Linacs, the undulation of electrons are done by strong stationary magnets [18]. However, the large intensities currently available in the laser lab means that an optical undulator provides a more compact and potentially effective means of enhancing the energies generated by the synchrotron. Compton (or Thompson in the classical limit) scattering provides one of the key mechanisms by which lasers can begin to generate high energy photons. Relating the a_0 parameter back to synchrotron radiation, a number of key elements require slight modification. The laser wavelength is λ_l and its wavenumber $k_l = 2\pi/\lambda_l$. This means the frequency is $\omega_l = k_l c$ and energy $\varepsilon_l = \hbar\omega_l$. The relativistic laser intensity parameter a_0, can be directly related to the undulator strength parameter K_u simply as

$$K_u = a_0 = 0.855\sqrt{I[10^{18}\mathrm{w/cm}^2]\lambda_L^2[\mu\mathrm{m}]} \tag{7}$$

For equations 2 and 5, as the electromagnetic field carries out the role of an undulator, $\Omega_u = \omega_L$ and the number of undulator/wiggler elements is given by the number of photons absorbed by an electron N_{ABS} which is 1 when $a_0 < 1$ and up to a_0^3 for $a_0 > 1$ [11]. For a laser-driven scenario, the energy of the

emitted radiation is then given by:

$$\omega_B = \frac{4\gamma^2 \omega_L N_{ABS}}{1 + (\gamma\theta)^2 + \frac{a_0^2}{2} + 2\frac{N_{ABS}\chi}{a_0}} \tag{8}$$

Here ω_B is the boosted photon emitted by the undulator/wiggler. The two additional modifications seen in the denominator of equation 8 are $a_0^2/2$ which represents the depletion of the laser pulse as electrons propagate through it, and $2N_{ABS}\chi/a_0$ which introduces the χ parameter. χ is the ratio of the electric field strength of the pulse to the Schwinger limit of the field , a effect of quantum electrodynamics (QED) which indicates that given a strong enough field strength, a laser can produce electron-positron pairs from a vacuum ($E_L = 1.3 \times 10^{18}$ Vm^{-1}[19]). As an electron possess an electric field, it too can contribute to this effect such that in practical units $\chi \approx 6.1 \times 10^{-6} \gamma a_0$. The first correction becomes significant at $a_0 > 1$ i.e., the wiggler regime however, the second correction is very much a QED consideration and need only be considered at extreme intensities or ultra-high relativistic velocities [11].

In order to build a compact γ-ray source, it is thus necessary to minimise the size of the electron accelerator. Laser wakefield acceleration (LWFA) can now give this opportunity, since they can sustain accelerating gradients of the order of 100's GVm^{-1} [20], reducing GeV-scale accelerators down to a few cm in length. The electrons accelerated in these fields are produced in extremely short bunches in the order of the plasma wavelength, with durations of τ_p (which is the plasma timescale [21]) [20]. When an ultra-

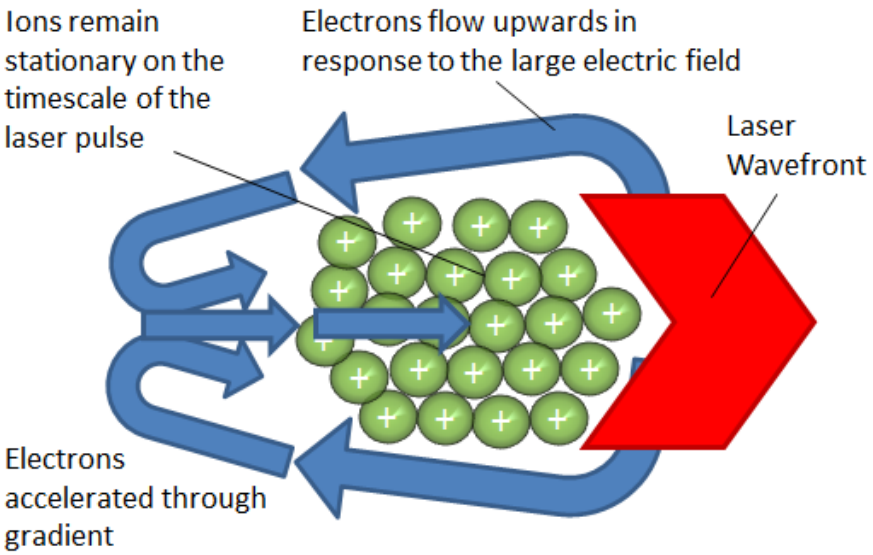

FIG. 4: A simplified diagram of the process of LWFA. The laser pulse arrives into the plasma, driving electrons out of its path. The heavier ions remain and create an enormous potential difference which accelerates the electrons to relativistic velocities behind the laser.

short, relativistically intense laser pulse propagates through an underdense plasma ($(\lambda_l/\lambda_p)^2 \ll 1$ whereλ_p is the plasma wavelength [21]), the field associated with the laser pulse envelope will drive electrons away from the pulse leaving a positively charged channel around the axis (see figure 4). The strong charge imbalance will drive the electrons back on-axis, effectively setting a longitudinal plasma wave with a strong electric field. Electrons injected into these waves are then accelerated in the longitudinal directions, with typical energies in the multi-MeV up to GeV [20].

As an example, figure 5 shows the fluorescence observed on a Lanex screen [22], and related electron spectra for a range of gas pressures (50, 80, 100 and 200 mbar) [23].

It can be seen that there is an optimum pressure for each setup that can generate high-energy, high-quality beams. Intuitively, the gas must be dense enough to generate the accelerating gradients, while not being so dense that the laser group velocity is reduced sufficiently so as to allow de-phasing to occur and destroy the wakefield [20].

The current record for the highest energy of laser-driven electron beams is held by the BELLA laser

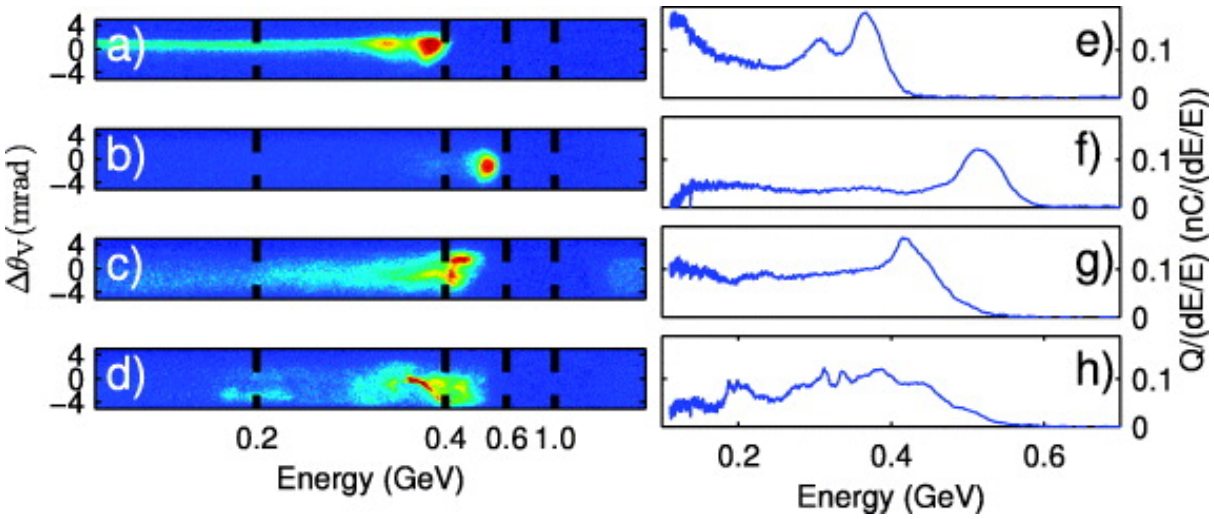

FIG. 5: Examples of raw electron energy spectra $(a-d)$ showing the fluorescence observed on a Lanex screen [22], and spectra in units of charge per relative energy spread $(e-h)$. These were observed ad a range of pressures from $50, 80100$ and 200 mbar of gases [23].

[24], which has accelerated electrons up to 4.2 GeV in 10 cm of guiding capillary shown in figure 6 [25].

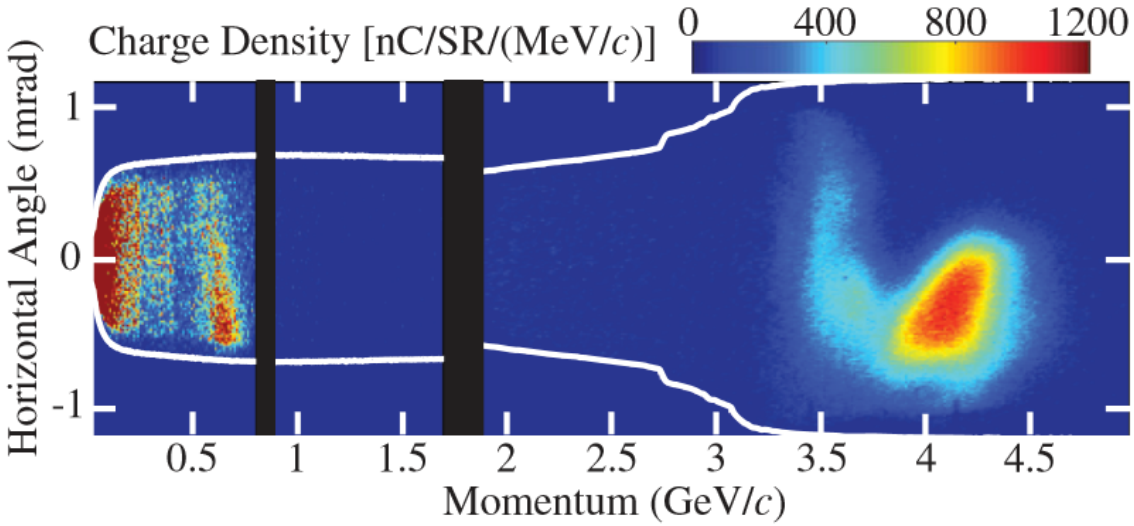

FIG. 6: The state of the art LWFA can produce 6 pC beams with an energy spectrum which reaches a 4.2 GeV by employing the use of capillary tubes as waveguides [25].

III. THE APPLICATION OF LASER BASED SYNCHROTRONS

Exploiting the undulations imposed by the laser on the electrons in LWFA as a source of high energy photons has already yielded some excellent results. This 'betatron' radiation leads to coherent and bright sources of x-rays presented in figure 7 [26, 27]. These sources imply a brilliance exceeding 10^{22} photons s^{-1} mm^{-2} mrad $^{-2}$ 0.1% BW. However, the energies are typically below 1 MeV. While the energies reported in current literature fall below those needed for the applications outlined at the beginning of this article, their usefulness should not be understated. Betatron sources from electrons generated via LWFA have

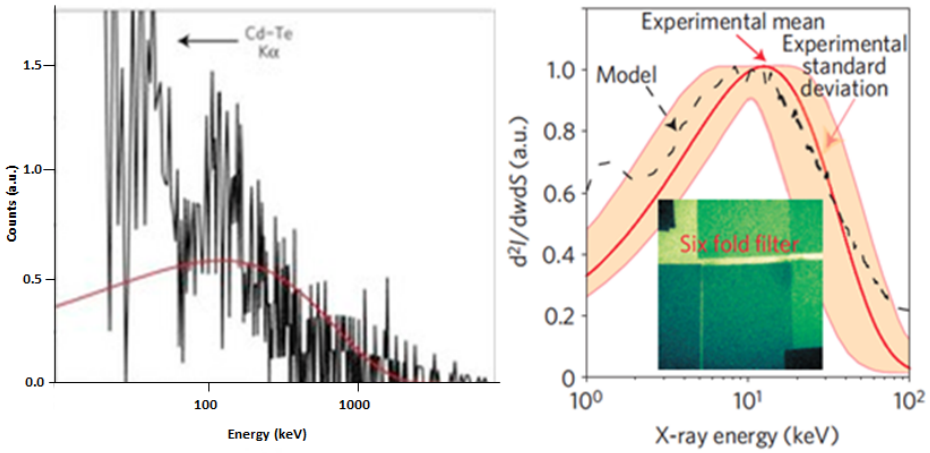

FIG. 7: Results presented in manuscripts regarding betatron sources from electrons generated via LWFA [26, 27]. These sources exhibit Micron scale source size are temporally coherent, of short duration and high flux.

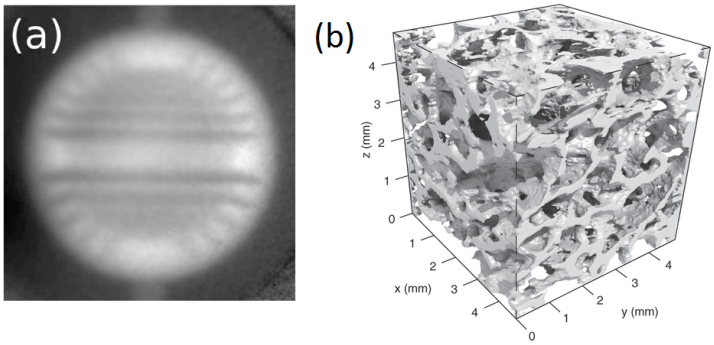

FIG. 8: A comparison of a Bremsstrahlung source (a) and a betatron source (b) for imaging. For the Bremsstrahlung source, the lack of coherence makes it difficult to obtain a high level of detail of the object being imaged, while the bright coherent betatron source allows one to generate detailed images of complex objects. In this case, a 3-D image of a human bone is able to be generated by stacking multiple images taken with an x-ray camera. Unlike conventional Bremsstrahlung based x-ray machines found in most hospitals, the betatron based source provides increased levels of details about the micro-structure of the bone [28].

been used to produce 3-D tomographic images of human bone and because conventional radiographs can not reveal detailed information about the micro-structure despite its importance as an indicator of osteoporosis [28]. When the results of such a source are compared with those of a Bremsstrahlung source such as that found in ref [12], it is easy to see the benefits. Figure 8 makes such a comparison. (a) demonstrate the imaging of a Bremsstrahlung source and (b) that of the betatron source. Clearly the betatron source can give extremely high resolution due to its coherence.

In order to boost the energy of photons emitted by the electrons, a second laser pulse can be used as an undulator as discussed in the previous section. For a counter-propagating geometry, as an ultra-relativistic electron advances through an intense laser field, the intensity of the laser enhances the frequency of photons generated as seen in equation 8 [11, 13, 17].

Work in this field is already under way and various groups have demonstrated successfully the generation of high energy photons from optical interactions. As an example of the possible results that can be obtained in this configuration, we show in Fig.9 a typical spectrum obtained during the interaction of a low energy electron beam with a low-intensity laser beam ($a_0 < 1$). The brilliance obtained in this experiment was of the order of 3×10^{18} photons s^{-1} mm^{-2} mrad^{-2} per 0.1% BW [29].

Figure 9 shows that for the undulator regime, the pattern of the photons generated follows closely that of the electron spectra. This is typical of the linear nature of the interaction. With γ_{max} = 160 for

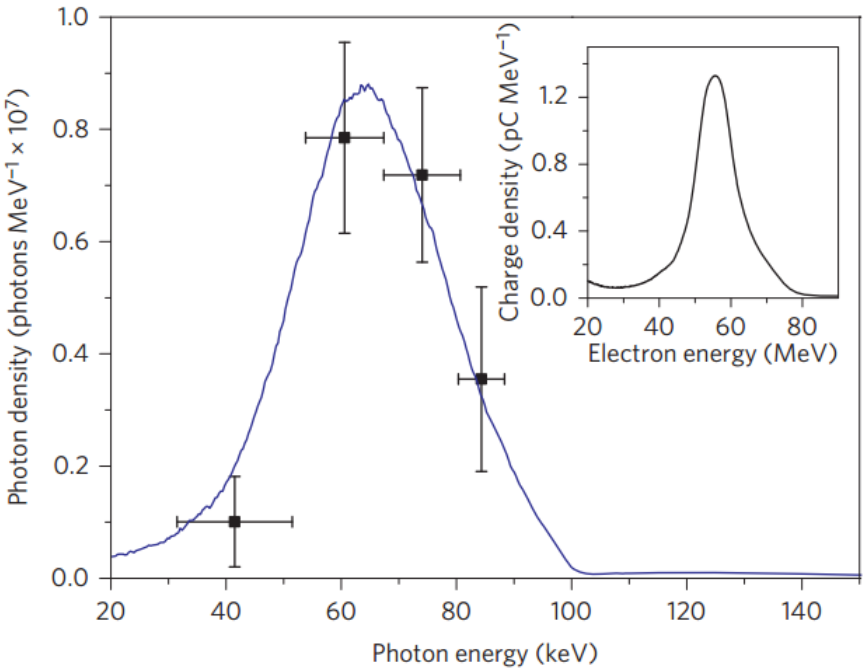

FIG. 9: X-ray spectral distribution (black squares) measured, for a single shot, by the Ross-filter pairs. Horizontal error bars represent the spectral width of the filter pair; vertical error bars represent the measurement error. The simulated X-ray spectrum (solid line), obtained from the experimentally measured electron-beam spectrum (inset), is normalized by dividing by a factor of 1.4.[29].

the electrons and a laser intensity $a_0 \approx 0.25$, the peak energy of the photons produced is 60 keV [29].

As all-optical Thomson source continues to be refined, the intensity becomes sufficient for exploration of the onset of the non-linear regime [30]. This effect was seen, in the perturbative regime, in Ref [30]. Typical results obtained in that experimental campaign are shown in figure 10. Run-averaged spectra are shown in red, white lines show the expected x-ray spectrum for each averaged electron spectrum. The simulation was performed with simulation package SPECTRA 9.0, assuming an equivalent undulator model with a peak undulator parameter of $K_u = a_0 = 0.9$ [30]. One can see a strong correlation between the theory and results obtained.

Exploring the properties of an all optical Thomson source is producing tunable and quasimonochromatic Thomson X-Ray sources and with continued refinement into the technique, the intensity becomes sufficient for exploration of the onset of the non-linear regime [30]. Previous investigations of laser-driven Thomson scattering have mostly focused on the linear or single-photon or undulator regime i.e., whenever the relativistically invariant dimensionless amplitude of the laser pulse ($a_0 < 1$) [29, 31] and report on γ-ray energies ranging from a few hundreds of keV [29] up to $3-4$ MeV [31]. Perturbative non-linear corrections ($a_0 < 1$) were first reported in Ref. [32]. Liu and collaborators recently reported on an increase in photon energy (up to $8-9$ MeV) by frequency converting the scattering laser up to its second harmonic (thus increasing $\hbar\omega_L$) [33]. However, using a higher laser frequency for scattering significantly reduces the laser energy available (crystal conversion efficiency into second harmonic of the order of $30-50$ %), and the laser a_0 implying a modest number of generated photons ($\approx 3\times10^5$ photons per shot are theoretically inferred in reference [33]). This relatively low number can be easily understood if we consider that it would scale as $N_\gamma \propto a_0^2$ for $a_0 \ll 1$ [17]. The brilliance of this source is thus not higher than laser-driven bremsstrahlung source [12, 34, 35] (see Fig. 16 for a comparison of reported brilliance for different γ-ray sources). Laser driven non-linear Thomson scattering ($a_0 \approx 1.5$) has been achieved using a single laser to both drive and scatter the electrons [36]. This generated γ-rays with energies of the order of few hundreds of keV but the single-laser setup makes it unfeasible to scale the system to higher photon energies.

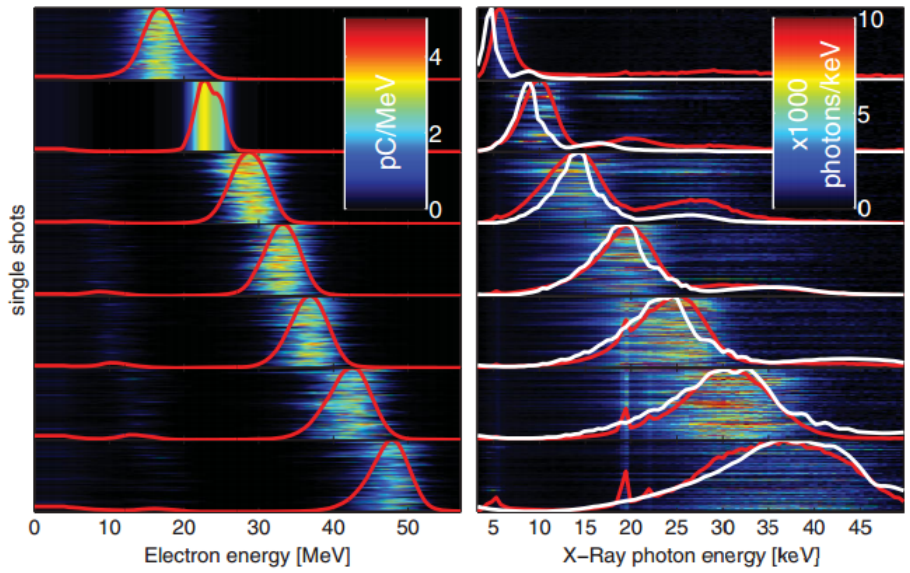

FIG. 10: The electron are presented on the left and corresponding photon spectra on the right. Each horizontal trace shows a single laser shot. Run-averaged spectra are shown in red, white lines show the expected x-ray spectrum for each averaged electron spectrum. The simulation was performed with SPECTRA 9.0, assuming an equivalent undulator model with a peak undulator parameter of $K_u = a_0 = 0.9$ [30].

IV. EXPERIMENTAL TECHNIQUES

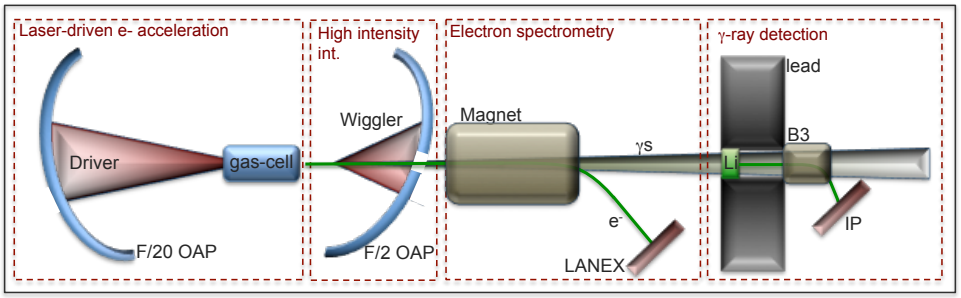

FIG. 11: Sketch of the experimental setup: an intense laser pulse (*Driver*) is focussed by an F/20 off OAP at the edge of a gas-cell to generate an ultra-relativistic electron beam (first box: *Laser-driven* e^- *acceleration*). A second, more intense laser pulse (*Wiggler*) is focussed by a holed F/2 OAP in a counter-propagating to the electron beam (second box: *High intensity int.*). After interaction, the electron beam is deflected by a strong pair of magnets onto a LANEX scintillator screen (third box: *Electron spectrometry*) whilst the generated γ-ray beam propagates up to a Li-based spectrometer (fourth box: *γ-ray detection)*. An F/15 hole in the F/2 OAP ensures unperturbed propagation of the scattered electron beam and generated γ-ray beam onto the detector, and minimises back-reflection of the laser in the amplification chain [16].

The results presented in the previous chapter show that an all-optical source of high energy is in fact possible to achieve. However, the number of photons and energies achieved can be enhanced if $a_0 > 1$. Using the Astra-Gemini laser, hosted by the Rutherford Appleton laboratory [37], which delivers two laser beams each with central wavelength $\lambda_L \approx 800$ nm, pulse duration $\tau_L \approx (42 \pm 4)$ fs, and energy after compression of 18 J, a recent experimental campaign demonstrated that the onset of non-linear Thomson scattering with $a_0 > 1$ is in-fact achievable. The setup used is presented in figure 11 [16].

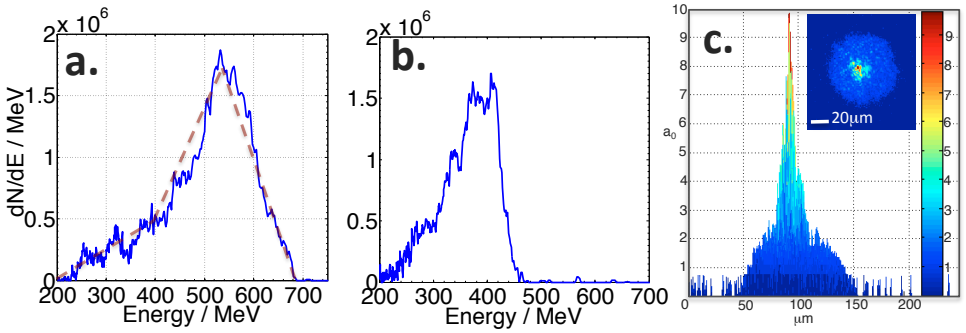

FIG. 12: **a.**,**b.** Electron spectra used for the first and second series of experiments, respectively. In frame a., the dashed red line represents the approximated electron spectrum used as an input for the theoretical calculations. **c.** Measured intensity distribution of the laser used for scattering (*Wiggler* in Fig. 11).

Using the two beam geometry, one pulse is able to take the role of a driving pulse. This pulse was focussed, using an F/20 Off-Axis Parabola (OAP). A quasi-monoenergetic electron beam with peak energy $E_{e^-} \approx 550$ MeV were consistently produced (typical examples of which are presented in figures 12(a) and (b)).

The second laser pulse assumed the role of wiggler and was focused using an F/2 OAP. This parabolic mirror had an F/15 hole in the middle, 1 cm downstream of the exit of the gas-cell which allows the electrons to travel through the mirror without impacting onto it and produce spurious noise.

A random spatial diffuser was inserted prior to the parabola in order to match the electron beam transverse size with the high intensity focus of the laser which was given as $a_0 = 2$. A peaked region with $a_0 = 10$ is also present FWHM ≈ 3 μm (the beam profile is presented in figure 12(c)). Further detail are presented within Ref. [16].

The main problem which needs to be solved is the issue of synchronising such ultra-short pulses to within a few fs of each other; the difficulty arises from the fact that this timescale is many orders of magnitude below the typical response time of modern electronic devices (which can respond on the 100's ps scale). In order to achieve synchronisation on the fs timescale, an interferometric technique was developed that allows one to synchronise pulses with a high level of precision (details of which can be found at [38]). As an example, we plot in Fig. 13 the effect of changing the time delay between the pulses onto the CCD detector.

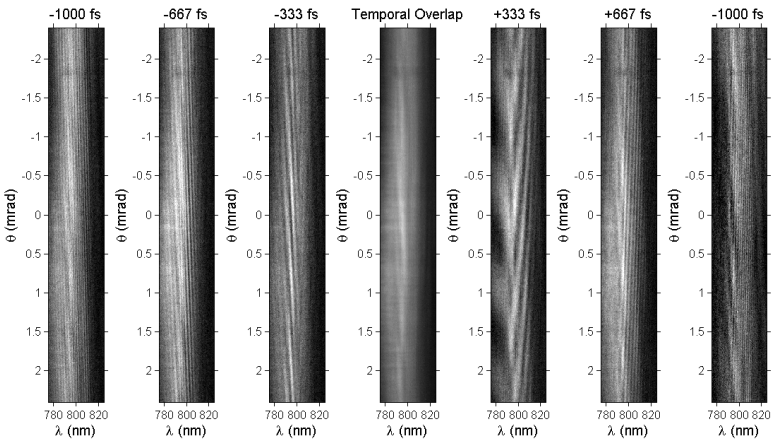

FIG. 13: The synchronisation process as seen on the CCD. Details in the text and in Ref. [38]

The images show the position on the CCD chip in the vertical axis against the wavelengths mapped to the CDD chip. The images moving from left to right demonstrate the changing pattern when the delay is changed in steps of $2T_0$ where T_0 is the laser pulse duration i.e., 45 fs. As can be seen the number of fringes seen in the horizontal axis falls as synchronisation is approached [38].

After synchronisation is accomplished, the setup given in figure 11 can be used to give simultaneous information on the electron and gamma ray spectra. Downstream of the F/2 OAP, the magnet (B = 1 T, length of 15 cm) deflects the electrons away from the generated γ-ray beam to a LANEX [22] scintillator, resolving electron energies from 120 MeV to 2 GeV.

By estimating the average energy $\mathcal{E}_{e^-}$ emitted by an electron with an energy of 550 MeV from the Larmor formula [14], we obtain $\mathcal{E}_{e^-} \sim 11$ MeV such that radiation-reaction effects are also negligibly small. The electron spectrum after the interaction is substantially unchanged (recoil-less interaction) and it can thus be used as a valid approximation for the initial electron spectrum.

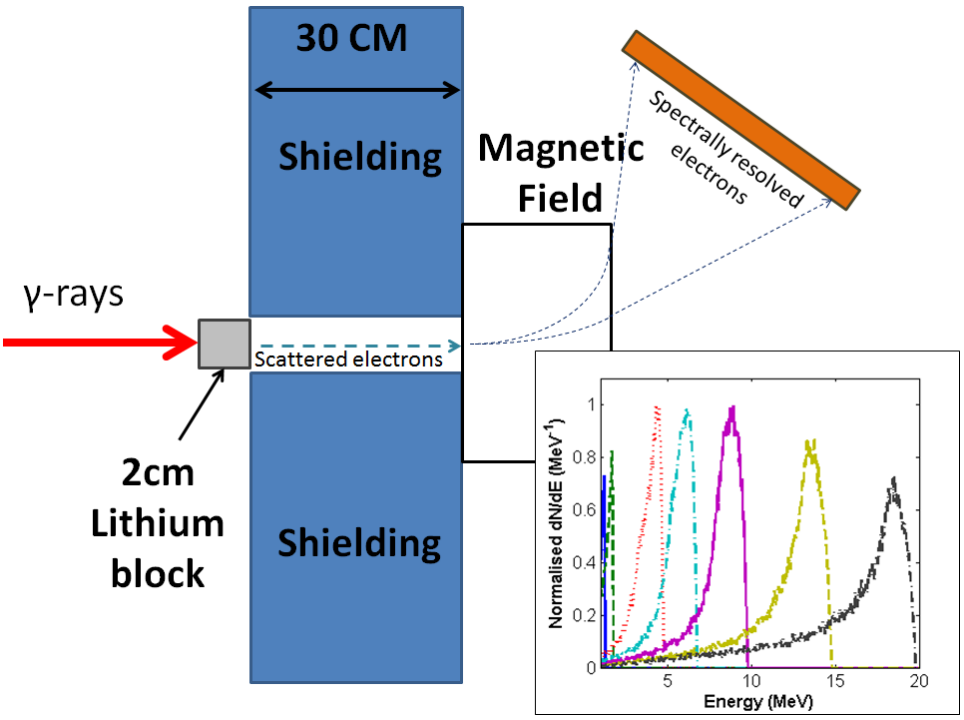

FIG. 14: The setup of the γ-ray detector. A 2 cm thick block of Li allows for the generation of secondary electrons via Compton scattering. The on-axis scattered electron population is angularly selected by a lead shield which also reduced the signal to noise ratio. A 0.3 T magnet resolves the electron population which is detected by an image plate [39, 40]. The graph shows the spectral shapes that are obtained for monoenergetic pencil beams of γ-rays of energies 1.5 (dark blue), 2 (green), 5 (red), 7 (light blue), 10 (purple), 15 (yellow) and 20 (black) MeV. Response of lithium to γ-ray beams is found at NIST [41] and more detailed findings of the detector are presented in reference [42].

For the γ-ray detection, a novel system based on Compton interactions with the electrons of lithium was employed; this system allows one to spectrally resolve high flux γ-ray beams (see figure 14 and reference [42]). Outside the main chamber, a 2 cm thick block of Li (transverse size of 5 mm) was inserted in the γ-ray beam path to allow for the generation of secondary electrons via Compton scattering. This angular acceptance was explicitly chosen to be comparable to the theoretically predicted angular spread of the γ-ray photons: $\theta_\gamma \approx a_0/\gamma_{e^-} \approx 2$ mrad. The on-axis scattered electron population retains the spectral shape of the γ-ray beam with an energy resolution of the order of the MeV. A 0.3 T, 5 cm long pairs of magnets spectrally dispersed the secondary electron beam onto an absolutely calibrated Imaging Plate [39, 40]. This spectrometer was encased into a 30 cm thick box of lead to minimise noise arising from off-axis scattered electrons and photons and from bremsstrahlung photons emerging from the dumping of the primary electron beam. Typical spectral resolution, as resulting from the interplay of the magnetic spectrometer resolution and uncertainty introduced by the deconvolution process, was of the order of $10-15\%$ whereas the uncertainty in yield was of the order of 10%. This system allowed us for the first

time to measure the absolutely calibrated spectrum of the generated γ-ray beam, in an energy window between 6 and 20 MeV and an energy resolution of the order of 1 MeV (full details can be found at [42]).

V. RESULTS

Examples of the electron spectra generated in the arrangement presented previously are given in figures 12(a) & (b).

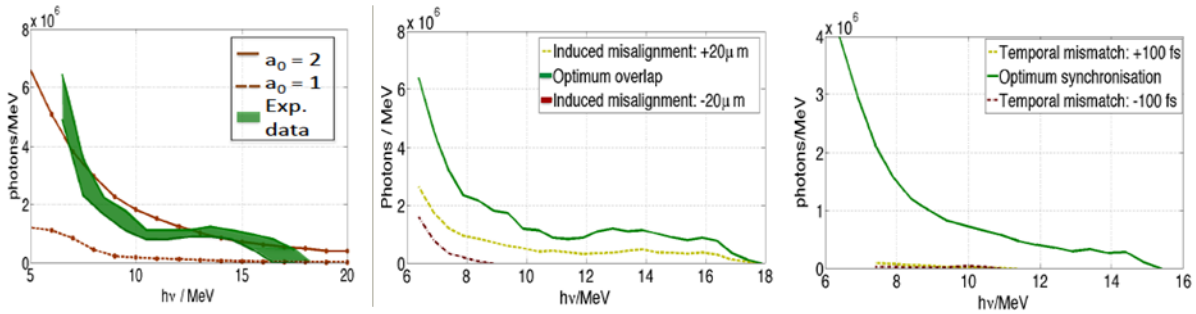

FIG. 15: The γ-ray spectra from NLTS as presented in reference [16]. **a.** green band: γ-ray spectrum as measured during the interaction of the laser-driven electron beam (spectrum depicted in Fig. 12.a) with the high-intensity focal spot of a secondary laser beam (spatial distribution shown in Fig. 12.c). The band represents the uncertainty associated with the experiment, as mainly resulting from the spectral resolution of the γ-ray spectrometer and the response of the detector. Solid and dashed brown lines depict theoretical expectations for the same electron and laser parameter as the experimental ones but with $a_0 = 2$ and $a_0 = 1$, respectively. **b.** The green line represents the measured spectrum for optimised electron-laser overlap (same as green band in frame a.) whereas dashed curves depicts the measured spectra if an artificial misalignment of ± 20 μm is introduced. **c.** The green line represents the measured spectrum for optimised electron-laser synchronisation (for an electron spectrum as the one in Fig. 12.b) whereas dashed curves depict the measured spectra if an artificial desynchronisation of ± 100 fs is introduced.

In conditions of best overlap and synchronisation between the electron beam and the laser pulse, this run produced a γ-ray beam with a monotonically decreasing spectrum, with a typical number of photons per MeV exceeding 10^6, extending up to $15-18$ MeV (green band in figure 15(a). The number and peak energy of the measured γ-ray photons is in good agreement with synchrotron calculations for $a_0 = 2$ (see figure 15(a). An induced spatial misalignment of $\pm 20\mu$m significantly reduces the signal whilst roughly preserving the same spectral shape (figure 15(b). No signal can be recorded if the misalignment is increased to $\pm 40\mu$m.

The dependence of the spectrum on the temporal overlap between the laser-accelerated electron beam and the undulating pulse is shown in figure 12. The γ-ray spectra shown in figure 15(c) show that changing the relative delay of the lasers by ± 100fs reduces the signal fall virtually to zero. It is thus clear that the observed γ-ray beam exclusively results from the electrons undulating in the laser field.

The source size is comparable to the electron beam diameter at interaction ($D_\gamma \approx (30 \pm 3)\mu$m), whilst the upper limit for the divergence of the measured photon beam is given by the angular acceptance of the γ-ray spectrometer (2.5 mrad). We can then assume the temporal duration to be comparable to that of the electron beam i.e., of the order of half plasma period in the acceleration stage [47] (≈ 30 fs for a plasma period of $\tau_{\rm pl} \approx (60 \pm 2)$ fs); in a 0.1% bandwidth around 15 MeV the approximate number of photons is $(3.0 \pm 0.2) \times 10^4$, implying a lower limit for the peak brilliance of $(1.8 \pm 0.4) \times 10^{20}$ photons s^{-1} mm^{-2} mrad^{-2} 0.1% BW. This brilliance is the highest ever achieved in a laboratory for multi-MeV γ-ray sources exceeding by several orders of magnitude that achieved by bremsstrahlung sources (see figure 16).

These parameters, namely the ultra-high brilliance and the short duration, are particularly appealing for practical applications such as radiobiology and active interrogation of materials. Typical cancer treatments are designed to deliver about twenty different fractions, each with a dose in the order of 1 Gy [48]. Modern commercial Linacs are designed to be able to deliver up to 30 Gy min^{-1} with a peak dose rate of 10^6 Gy min^{-1} [49]. For the present work, simulations using the Monte Carlo scattering

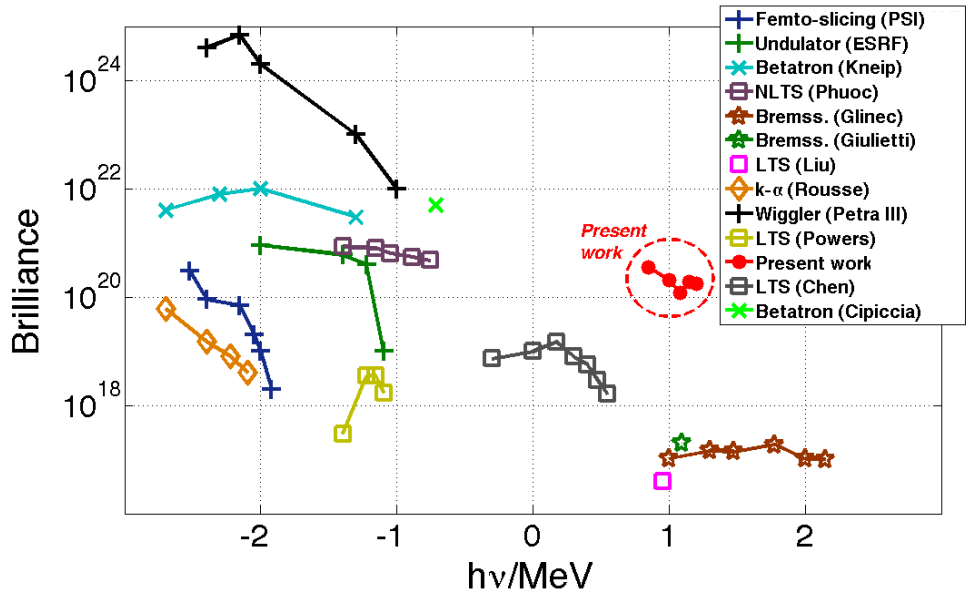

FIG. 16: Comparison of the present γ-ray source (solid red circles) with other generation mechanisms reported in the literature: free-electron laser (PETRA III, black crosses, [43]), k-α (orange diamonds, [44]), solid-state undulators (ESRF, green crosses [45] and PSI, blue crosses [46]), betatron radiation (light blue crosses [27]), bremsstrahlung radiation (green stars [34] and brown stars [12]), non-linear relativistic Thomson scattering (NLTS, dark purple squares [36]), and linear relativistic Thomson scattering (LTS, yellow squares [29], grey squares [31], and light purple square [33]). Brilliance is expressed in units of photons s^{-1} mm^{-2} $mrad^{-2}$ 0.1% BW

code FLUKA [50, 51] indicate that at 40 cm from the γ-ray source that a mm scale water target would absorb a dose of 0.2 Gy which implies a dose rate of $\approx 2 \times 10^{13}$ Gy s^{-1}, the highest ever achieved in the literature. This laser-driven source will then allow for studies of non-linear response of living tissue to radiation on a femtosecond scale. Moreover, the inherently compact nature of this all-optical source means that scanning for special nuclear materials is now viable. With a photon number of $\approx 10^7$ delivered in a 10's of fs, the flux ($\approx 10^{21}$ photons s^{-1}) greatly exceeds the requirements for the study of nuclear dipole resonances and photofission of $\approx 10^{13}$ photons s^{-1} in a 10% bandwidth. Even when compared with state of the art machines such as HIGS in Carolina USA [52], which produces γ-ray beams with $\approx 10^7$ photons s^{-1}, this source could represent a huge leap forward in the realisation of the scanners for shipping containers outlined in the first section.

VI. CONCLUSION & OUTLOOK

The demonstration of an optical and compact source of bright and multi-MeV γ-rays, provides a unique opportunity for studies in nuclear physics to be carried out in laser laboratories. As work is in its infancy, there is much scope for development which will lead to the compact-scale production of high quality γ-ray beams for use in the medical industry and the non-invasive scanning of shipping containers.

However, the spectra produced (hinted at in equation 4) when moving into the non-linear intensity regime remains an issue that needs to be tackled. Equation 9 gives the expected bandwidth:

$$\frac{\Delta\omega_B}{\omega_B} \approx \sqrt{\left(\frac{2\Delta\gamma}{\gamma}\right)^2 + \left(\frac{\Delta\omega_L^2}{\omega_L}\right)^2 + \left(\frac{a_0^2}{2}\right)^2} \tag{9}$$

The first term shows the importance of obtaining high energy mono-energetic sources of electrons through LWFA while the second term relates to the bandwidth of the laser itself. This latter term is generally small and does not make a significant contribution to the broadening when compared to the other

terms. The final term demonstrates that at high intensities, as the electron emits continuously during its interaction with the laser field, the stronger the field, the wider the bandwidth. While it may seem like this is a problem that cannot be resolved, it has been recently proposed that a suitable chirp of the scattering laser might minimise this issue. An example of these theoretical predictions can be found in Ref. [53] (see Fig. 17 for an example of these calculations).

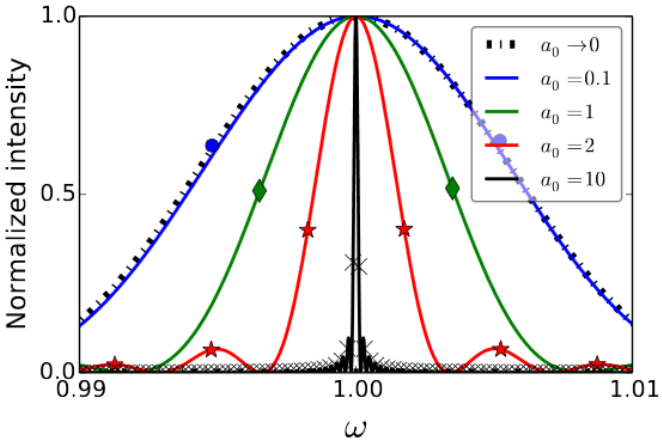

FIG. 17: The graph shows the normalised intensity against the normalised frequency of the emitted photons. It can be seen that at higher values of a_0, the correct chirping of the laser pulse can greatly suppress the harmonics that would otherwise be generated [53].

For now, research needs to be continued and work is already underway to develop further the LWFA technique. As well as better quality electron beams, more intense lasers will of course, be a welcome addition to the field allowing higher intensities larger focal spots with which to interact. As well as trying some of the methods outlined in Ref. [53].

As a consequence of such promising results in the field, work has already began on the extreme light infrastructure (ELI) in Eastern Europe [54]. The ELI project aims to represent the pinnacle of laser science providing a peak power of 200 PW. Additionally, the ELI nuclear physics (ELINP) division in Romania will exploit the all-optical Compton source to provide users with a stable source of tunable, high-energy photons with energies in the order of 0.219.5 MeV and spectral density of $(0.8 - 4) \times 10^4$ ph $s^{-1}eV^{-1}$. This means that nuclear scientist can conduct experiments using a source with a peak brilliance $10^{20}10^{23}$ $s^{-1}mm^{-2}mrad^{-2}$ 0.1%BW [55, 56]. Already, users of the facility are planing to exploit this unique opportunity to conduct experiments in photofission [57] and particle core couplings in 'doubly magic' nuclei [58]. However, this is just the beginning of the possible applications of this type of all-optical source and with improvements in the LWFA technology being developed, there could be the opportunity to further enhance the energies achievable in this type of arrangement.

ACKNOWLEDGEMENTS

D.J. Corvan and G. Sarri wish to acknowledge the financial support from EPSRC (grant number EP/L013975/1).

[1] W. Bertozzi *et al.* Phys. Rev. C, **78**, 041601 (2008).
[2] Nuclear fluoresence. "`http://www.tunl.duke.edu/groups/nnsa/nrf.html`".
[3] D Doré *et al.* J. Phys.: Conf. Ser., **41**, 241 (2006).
[4] J. Frittelli. Port and Maritime Security, Background and issues for Congress, CRS Report RL31733, US Library of Congress, (2005).
[5] Csi: Container security initiative. `http://www.cbp.gov/border-security/portsentry/cargo-security/csi/csi-brief`.

[6] J.M. Hall *et al.* Nucl. Inst. Meth. Phys. B **261**, 337, (2007).
[7] D.R. Slaughter *et al.* Nucl. Inst. Meth. Phys. B **241**, 777, (2005).
[8] E. B. Podgorsak. Radiation Oncology Physics: A Handbook for Teachers and Students*, IAEA, Wien 2005.*
[9] K.J. Oxford. Nature **267**, 103, (1977).
[10] Fermi Gamma Telescope. "http://fermi.gsfc.nasa.gov/".
[11] Di Piazza *et al.* Rev. Mod. Phys. **84** 1177 (2012).
[12] Y. Glinec *et al.* Phys. Rev. Lett. **94**, 025003 (2005).
[13] A. Hofmann. The Physics of Synchrotron Radiation*, Cambridge University Press, 1 edition, 2004.*
[14] J. D. Jackson. Classical Electrodynamics*, Wiley, 3rd edition 1998,.*
[15] Diamond Synchrotron. "`http://www.diamond.ac.uk/Home/About/FAQs/About-Synchrotrons.html`".
[16] G. Sarri *et al. Phys. Rev. Lett. **113** 224801 (2014).*
[17] S. Corde *et al.* Rev. Mod. Phys. **85**, 1 (2013).
[18] D. I. Thwaites and J. B. Tuohy. Phys. Med. Biol. **51**, R343 (2006).
[19] Lifshitz Beresteetskii and Pitaevskii. L. D. Landau and E. M. Lifshitz Quantum Electrodynamics*, volume 4, Pergamon Press, 4 edition, 1980,.*
[20] E. Esarey *et al.* Rev. Mod. Phys. **81**, 3, 1229 (2009).
[21] R. Dendy. Plasma Physics An Introductory Course*, volume 1. Plasma Physics, Cambridge University Press, 1 edition, 1996.*
[22] Y. Glinec *et al.* Rev. Sci. Instrum. **77**, 103301, (2006).
[23] T. P. A. Ibbotson *et al.* New Journal Phys. **12**, 045008 (2010).
[24] W. P. Leemans *et al. Proceedings of PAC2013, Pasadena, CA, 1097, (2013).*
[25] W. P. Leemans *et al. Phys. Rev. Lett. **113**, 245002, (2015).*
[26] S. Cipiccia *et al.* Nat. Phys. **7**, 867 (2011).
[27] S. Kneip *et al.* Nat. Phys. **7**, 737 (2012).
[28] J. Cole *et al.* Nat. Comm. **5**, 13244 (2015).
[29] N. D. Powers *et al. Nat. Phot. **8** 28 (2014).*
[30] K. Khrennikov *et al.* Phys. Rev. Lett. **114**, 195003 (2015).
[31] F. F. Chen. Introduction to Plasma Physics and Controlled Fusion*, volume 1. Plasma Physics, Springer, 2 edition, 2006.*
[32] C. Bula *et al.* Phys. Rev. Lett. **76**, 3116 (1996).
[33] C. Liu *et al.* Opt. Lett. **39**, 4132 (2014).
[34] A. Giulietti *et al.* Phys. Rev. Lett. **101**, 105002 (2008).
[35] W. Schumaker *et al.* Phys. Plasmas **21**, 056704 (2014).
[36] K. Ta Puhoc *et al.* Nature. Phot. **6**, 308 (2012).
[37] C. J. Hooker *et al.* J. Physique IV **133**, 673 (2006).
[38] D.J. Corvan *et al.* Optics Express **24** 3127 (2016).
[39] B.R. Maddox *et al.* Rev. Sci. Instrum. **82**, 023111, (2011).
[40] K.A. Tanaka *et al. Rev. Sci. Instrum.* **76**, 013507, (2005).
[41] National institute of standards and technology. `http://www.nist.gov/`.
[42] D. J. Corvan *et al.* Rev. Sci Instrum. **85**, 065119 (2014).
[43] The flash laser system. "`http://flash.desy.de/`".
[44] A. Rousse *et al.* Phys. Rev. E **50**, 2200 (1994).
[45] Accelerators. "`http://www.esrf.eu/Accelerators/Performance/Brilliance/`".
[46] Psi. "`http://www.psi.ch/sls/microxas/femto/`".
[47] S. P. D. Mangles *et al.* Phys. Rev. Lett. **96**, 215001 (2006).
[48] T. S. Lawrence *et al.* Principles and Practice of Oncology. 8th ed. Philadelphia: Lippincott Williams and Wilkins, (2008).
[49] C.C. Ling *et al.* Radiatherapy & Oncology, **95** 261 (2008).
[50] A. Ferrari*et al.* CERN-2005-10 , INFN/TC 05/11, SLAC-R-773, 2005.
[51] S. Roesler *et al.* Computing in High Energy and Nuclear Physics 2003 Conference (CHEP2003), La Jolla, CA, USA, March 24-28, 2003.
[52] Higs. "`http://www.tunl.duke.edu/web.tunl.2011a.higs.php`".
[53] S.G. Rykovanov *et al.* ArXiv 1412.2517v1 (2014).
[54] Extreme Light Infrastructure. "`http://www.eli-beams.eu/`".
[55] Extreme Light Infrastructure Nuclear Physics. "`http://www.eli-np.ro/`".
[56] C.A. Ur *et al.* Nuclear Instruments and Methods in Physics Research B **355** 198 (2015).
[57] P. Constantin *et al.* Nuclear Instruments and Methods in Physics Research B **372** 78 (2016).
[58] S. Leoni *et al.* ACTA PHYSICA POLONICA B **46** 637 (2015).